Fingering and pressure distribution in lifting Hele-Shaw cells with grooves: A computer simulation study

Sujata Tarafdar,[1] Suparna Sinha,[1] Soma Nag,[1] and Tapati Dutta[2]
[1]*Physics Department, Condensed Matter Physics Research Centre, Jadavpur University, Kolkata 700032, India*
[2]*Physics Department, St. Xavier's College, Kolkata 700032, India*
(Received 7 April 2009; revised manuscript received 28 May 2009; published 26 August 2009)

We report a computer simulation study of viscous fingering patterns in a lifting Hele-Shaw cell with grooves. Here circular or square grooves concentric to the plates are etched on the lower plate. Experiments show that the presence of such grooves affect formation of viscous fingers quite strongly. We report a simulated pressure map generated in such grooved cells, when the two plates are separated with a constant force and compare the patterns with experiments. Variation in the simulated patterns for different fluid viscosity and lifting force is also studied.

DOI: 10.1103/PhysRevE.80.026315 PACS number(s): 47.15.gp, 47.54.−r, 07.05.Tp

I. INTRODUCTION

The Hele-Shaw (HS) cell [1] is a simple apparatus for studying the instability developed at the interface of fluids of different viscosities, known as viscous fingering (VF) [2,3]. The normal HS cell consists of two glass plates separated by a small gap, containing the more viscous fluid. There is a hole in the upper plate, through which the less viscous fluid is forced into the cell [4].

The lifting Hele-Shaw cell (LHSC) is a modified version of the normal HS cell. Here, the plates are drawn apart, causing the less viscous fluid to enter from the sides. The more viscous fluid, sandwiched between the two plates, is displaced in the process and fingering patterns are formed at the interface [5–7].

The effect of anisotropy, introduced through patterns on the lower plate of the normal HS cell is well known [8–10]. Patterns on the lower plate also have a significant effect in LHSC [11]. The time of plate separation and pattern formation with circular grooves was reported in [11].

In the present paper we report experiments on LHSC with square grooves. Then we report a computer simulation code, developed for generating viscous fingering patterns in the LHSC with circular and square grooves and compare the resulting patterns with experiments.

With grooves etched on to the lower plate, the pressure distribution conforms to the symmetry of the grooves in addition to the overall radial symmetry of the setup and produces interesting changes in fingering patterns. Here we simulate grooved LHSC at a constant lifting force. The pressure distribution is mapped out and the contours of isobars and finger advancement are presented for LHSC without grooves as well as with grooves of different symmetry. It is seen that the qualitative features of the experimental VF formed with square and circular grooves is well reproduced. In the numerical model, the effect of the grooves is taken into account simply by imposing an equalization of the pressure along it. The rationale behind this is the observation in experiments, that once a finger reaches a groove, air immediately spreads all over the groove, equalizing the pressure along it. Even this simplified approach demonstrates the difference in the pressure distribution between plane and grooved plates. Differences in groove patterns also have a significant effect on fingering.

The HS and its variants serve as model systems for a number of practical problems. The disordered version of the HS cell [12] has been studied as a model for geological porous media and rough surfaces. The present grooved version may be considered as a model for fractured surfaces with channels. Opening up of cracked porous rocks, which may be partially saturated by one or more fluids can be modeled, along directions suggested from this study.

The LHSC is also an appropriate model for practical problems in adhesion [13–15]. The grooved LHSC can be used to study adhesion between rough or patterned surfaces. Different interesting modifications of the HS cell are reviewed in [16].

II. LHSC EXPERIMENT

The lifting Hele-Shaw cell consists of two plates of toughened float glass. The plates are 10 cm in diameter and 0.5 cm in thickness.

Initially a small volume of fluid measured accurately with the help of an accupipette is placed at the center of the stationary lower plate. For the grooved plates the fluid is placed at the center of the groove (as far as possible, since the process is manual). The upper plate, which is movable, is pressed on the lower plate carrying the blob of fluid. This creates a situation where a fluid having higher viscosity is surrounded by one with lower viscosity (air in this case) and the combination is sandwiched between two parallel plates. Then the upper plate is slowly lifted, with a constant force, keeping it parallel to the lower plate. An air compressor operating a pneumatic cylinder-piston controls the lifting force. The dynamic profile of the moving fluid—air interface is recorded by a charge-coupled device (CCD) camera, placed below the lower glass plate.

In this study, we report anisotropy in the setup, with etched patterns on the lower glass plate. Differences in patterns between (i) a plane glass plate, (ii) a plate with a circular groove and (iii) a plate with square grooves are experimentally recorded. Figure 1 shows patterns generated with this set up for the lower plate (A) plane, (B) circular

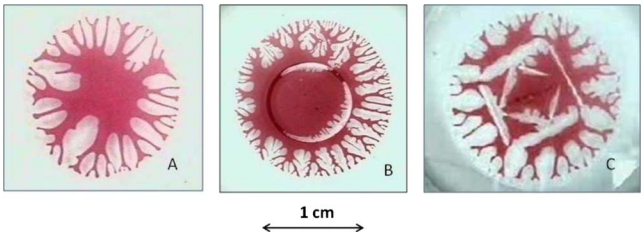

FIG. 1. (Color online) Experimentally obtained viscous fingers for (a) plane plate, (b) circular grooved plate, and (c) square grooved plate with a Newtonian fluid. The square groove has another smaller square groove inside rotated at angle 45° to the first. Secondary fingers can be seen starting from the grooves, where the air has spread very rapidly.

grooved, and (C) square grooved, with a Newtonian fluid—olive oil. The patterns with plane and circular grooved plates have been reported earlier in [11], they are included here for comparison with square groove plate patterns. The square grooved plate used here has two square grooves, the smaller one is etched inside the bigger and rotated 45°, with respect to it.

III. THEORY

In the normal Hele-Shaw cell, usually the invading fluid is air and is assumed to be nonviscous. The pressure distribution in the displaced fluid is obtained as a solution of Laplace's equation [2]. This results from a two-dimensional flow between two plates with a constant separation b.

$$\nabla^2 P = 0. \tag{1}$$

However, in the LHSC, the plate separation $b(t)$ becomes a function of time. The problem can still be considered as a quasi-two-dimensional problem, with P now a solution of Poisson's equation [17,18,15]. The idea is as follows: we look at an elementary area $da=dxdy$ at a position x,y on the plate. During lifting, we assign the volume occupied by the fluid $b(t)da$ to the cell at x,y. Here $b(t)$ is the height of the fluid column above da. As $b(t)$ increases, the effective fluid volume in the cell increases and Poisson equation becomes valid, rather than Laplace's. The source term in Poisson equation can be determined from the lifting conditions.

We follow essentially the approach of Thamida [15]. The z axis is taken normal to the plates and the fluid lies in the x-y plane. The boundary conditions are—the pressure at the interface of the displaced and invading fluid. This is the atmospheric pressure P_0. The pressure integrated over the whole area a of the displaced fluid is the constant lifting force $-F$,

$$\int P dx dy = -F. \tag{2}$$

Since the volume of the fluid, assumed incompressible is a constant V_0,

$$V_0 = a(t)b(t). \tag{3}$$

We start with the continuity equation for the incompressible fluid,

$$\nabla \cdot \mathbf{u} = 0, \tag{4}$$

where, $\mathbf{u}$ is the velocity of the fluid. i.e.,

$$\frac{\partial u_x}{\partial x} + \frac{\partial u_y}{\partial y} + \frac{\partial u_z}{\partial z} = 0. \tag{5}$$

Invoking the thin film lubrication approximation, assuming that u_z is independent of x and y, one has

$$\frac{\partial u_z}{\partial z} = \frac{1}{b}\frac{db}{dt}. \tag{6}$$

Darcy's law relates the lateral fluid velocity to the local pressure gradient as

$$u_x = -\frac{b^2}{12\mu}\frac{\partial P}{\partial x} \tag{7}$$

and a similar relation for u_y, here μ is the viscosity of the higher viscosity fluid. So, finally the two-dimensional Poisson equation to be solved is

$$\nabla^2 P = -\frac{12\mu}{a_0^2} a \frac{da}{dt}. \tag{8}$$

Here, a_0 is the initial area occupied by the higher viscosity fluid. We have written the equation in dimensional form, but we are at present making only a qualitative comparison of the patterns with experiments, so exact units and numerical values may be considered as arbitrary.

The above equations cannot be solved analytically, after the initial linear response regime. We solve the equations numerically, to simulate the growth of fingers, the details are given in the next section.

The presence of grooves makes the situation considerably complex. At present we consider one groove only, either circular or square. The presence of the groove is taken into account as an equalizing effect on the contour with the desired shape. Other factors, such as the change of fluid depth at the groove are ignored.

IV. COMPUTER SIMULATION ALGORITHM

In conformity with the symmetry of the setup, we formulate the problem initially in polar coordinates. The plates are considered to be circular with radius r. r varies from 1 to 24 and θ from 0 to 180. The polar coordinates of the system are then converted to Cartesian coordinates, through the relations

$$x = r\cos(\theta), \quad y = r\sin(\theta). \tag{9}$$

Only the integral part of x and y are retained. We have thus a circular arrangement of sites on a square lattice.

We introduce stochasticity in the form of a random initial disturbance along the boundary of the fluid blob. Each site on the circular boundary is given an indentation varying randomly between 0 and 3 units. These indentations represent fluctuations due to thermal noise, or surface irregularity and

may grow into a finger. We have repeated the simulation for at least ten different initial random configurations, for each parameter set, to check reproducibility of results.

A. Plane lower plate

In the case of a plane lower plate, the algorithm is as follows:

(1) Fluid sites occupying a circular area a_0 are marked by an index 1 and sites occupied by air are marked by 0.

(2) The boundary conditions are set as a constant pressure (atmospheric, taken as 0) at the outer periphery of the fluid and a negative value $-p_0=p00$ at the center. μ, a_0, and $p00$ are parameters determining the initial conditions.

(3) Laplace equation is solved, to get the initial pressure distribution and the pressure at each site is added to find the total lifting force $-F$. Darcy's law Eq. (7) is used to find the fluid velocity at each site, from the pressure gradient.

(4) The outer periphery is updated by allowing the fluid to move according to the velocity obtained in the previous step.

(5) Since F must be maintained constant, the pressure at the center $-p_0$ is increased in steps, until the pressure distribution is such that the condition, $\Sigma P(x,y)=-F$, is satisfied for the updated pressure $P(x,y)$ at each site.

(6) Now the pressure distribution is updated solving Poisson's Eq. (8) taking into account the new area. A suitable time interval δt is chosen as the unit of time, so $(a_{t+1}-a_t)/\delta t$ is the rate of change of area in Eq. (8). Each time the pressure distribution changes, the constant force condition $\Sigma P(x,y)=-F$ is re-established, by manipulating $-p_0$.

(7) Darcy's law is again invoked to get the fluid velocities, and steps 4 to 6 are repeated as long as necessary to map the evolving fluid boundary and hence the finger growth. To solve Laplace equation and Eq. (8), we use our own codes based on the formalism described in standard literature such as [19,20].

B. Grooved lower plates

We have simulated the fingering when there is a single circular or square groove etched on the lower plate. The simulation algorithm is as follows: we assume that the pressure along the groove is equal, i.e., there is an isobar having the shape of the groove in the system. The pressure on the isobar of course changes with time.

As already discussed, this is borne out by experiment. The experimental development of the fingers shows that spreading of air along the groove is extremely fast compared to finger growth in the plane region. Subsequently, growth of secondary fingers from the groove is preferred, growth of the other primary fingers being inhibited.

The details of the simulation algorithm for the grooved plate problem will be clear from the flowchart shown in Fig. 2. The essential modifications of the simulation algorithm are as follows. We initially calculate the pressure distribution from Laplace's equation with boundary conditions as before, forgetting about the groove. Then we calculate the average of the pressure over all the groove sites and reassign that average value to all groove sites.

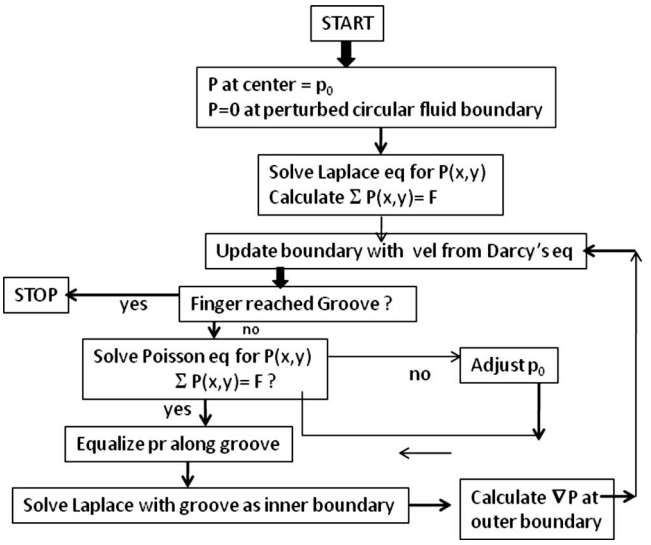

FIG. 2. Flowchart illustrating the sequence of steps followed for the simulation of the grooved patterns.

As before, the condition for constant lifting force is maintained through the condition $\Sigma P(x,y)=-F$, ensured by adjustment of p_0. In the lifting step, pressure is calculated from Poissons's equation, with the appropriate pressure at the center and groove pressure equalized as before. In the step when the fingers actually advance, according to Darcy's law, we use Laplace equation with the groove (having the equally distributed pressure previously determined) as the inner boundary and the outer fluid-air interface with 0 pressure as the outer boundary. Here Laplace is used instead of Poisson, since the increased height for this step has already been taken into account. These steps are repeated as long as at least one of the fingers touches the groove, refer to Fig. 2.

Patterns for circular fluid blobs of radius 24 and a circular groove of radius 8 have been simulated. For a plate with a square groove, exactly the same procedure is followed. The simulation is continued until the fingers reach the groove. The different colors correspond to decreasing pressure, starting from the outer boundary. The positions of the circular and square grooves are marked in black.

It is to be noted that, at each time step after the initial, the pressure $P(x,y)$ is calculated first from Poisson's equation, in order to get the average pressure along the groove. Force conservation is ensured, and then the pressure distribution is again calculated from Laplace equation with the groove as the inner boundary. This pressure distribution is used in Darcy's law to get the interface velocity. The actual advancement of the fingers, occurs of course, only once in a time step. At present, our system size is not very large, so the choice of the time interval δt becomes restricted. We choose the interval, which is large enough to produce a finite finger advancement, but is small enough to show several successive finger contours, before reaching the center. We have checked that system sizes up to 50, produce similar results. A detailed study of larger systems is in progress.

V. RESULTS AND DISCUSSION

One of our primary objectives is to see how the pressure variation within the fluid changes, when the upper plate is

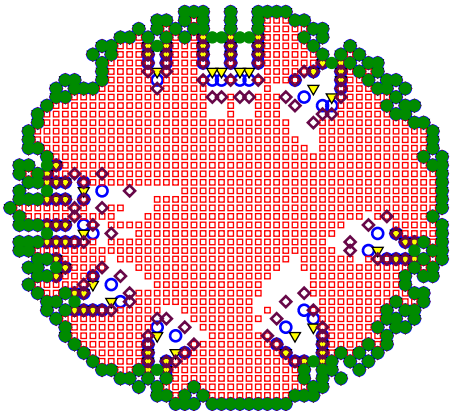

FIG. 3. (Color online) A viscous fingering pattern generated by simulation of the lifting process at constant force, with viscosity parameter 0.016 and initial pressure at center 14.6. The different symbols indicate the following—solid (green) circles mark the initial position of the fluid-air interface. Open symbols—triangle (yellow), circle (blue), and diamond (violet) mark the position of the advancing interface after 3, 4, and 5 steps, respectively. Squares (red) show the distribution of the displaced fluid after 6 steps.

lifted at a constant force. We have studied the development of fingers on a fluid blob of radius 24 units. The results we have presented are for μ=0.014–0.017. The initial central pressure $p00$, which determines the lifting force has been varied from 13 to 15. All parameter values are in arbitrary units. For still lower pressure there is no fingering. δt has been taken as 0.7, this makes the finger advancement length optimum. There is scope for variation of parameter combinations to look at larger sized systems.

We have chosen the parameter values such that about 5–10 time steps take the fingers to the center for the plane plate. Since fingers are advanced in discrete steps determined by the velocity, a velocity less than 1, means no advancement in that step.

A. Plane plate

Advancement of the fingers at different time steps is shown in Fig. 3. For the plane plate with no grooves it took 6 time steps for the fingers to reach the center in this particular realization.

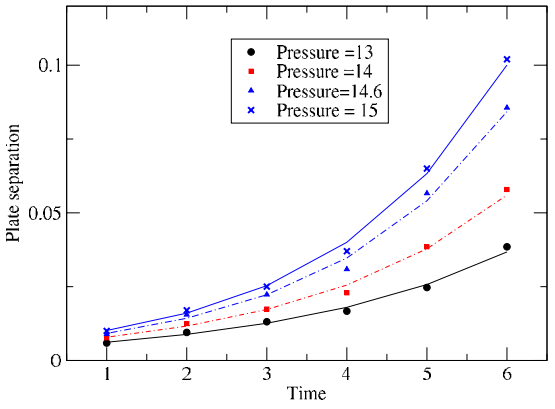

FIG. 4. (Color online) Simulated plate separation as function of time for several lifting pressures are represented by the symbols, the lines are exponential fits. All quantities are in arbitrary units.

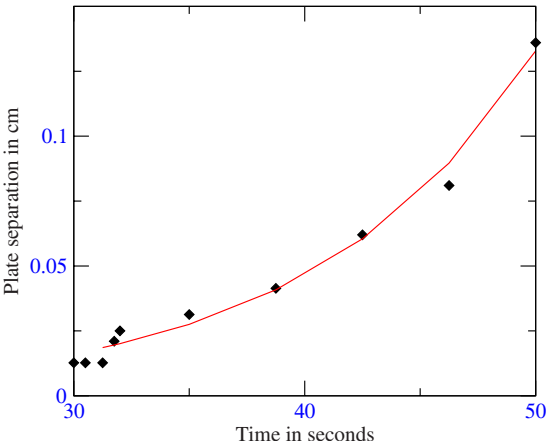

FIG. 5. (Color online) Experimental plate separation as function of time is represented by the symbols, the line is the exponential fit.

The plate separation at each time step can be calculated from the inverse of the area covered by the fluid, since the volume of fluid is constant. We find that the separation increases exponentially, some results are shown in Fig. 4.

Interestingly, the experimental results also show an exponential increase [21], though this is not predicted from theory [15]. Experimentally obtained plate separation, also calculated from volume divided by area of contact of fluid, as a function of time (averaged over five experiments) is shown in Fig. 5. The exponential fit is also shown. Figure 6 shows the variation of the fluid area of contact, as function of μ. For smaller μ, fingers penetrate more and the area of contact decreases strongly. Simulations for each set of parameters have been done for ten different random initial configurations, and average results are presented here.

The simulated pressure distribution in the plane plate with no grooves is shown in Fig. 7. The different colors (shades) represent ranges of pressure with a difference of 1 in arbitrary units. The pressure at the boundary is 0 and at the center it is −30.

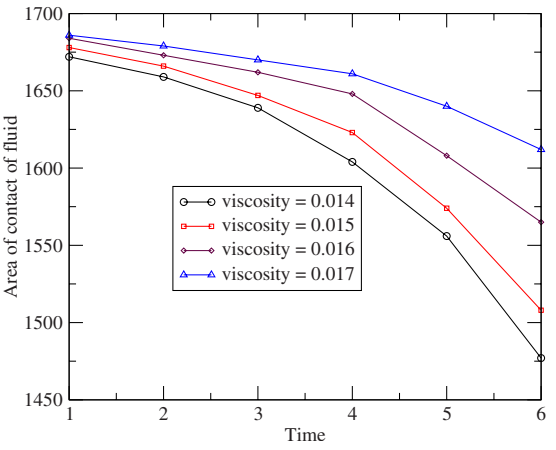

FIG. 6. (Color online) Simulated area of contact of fluid, as function of time for varying viscosity is shown. All quantities are in arbitrary units.

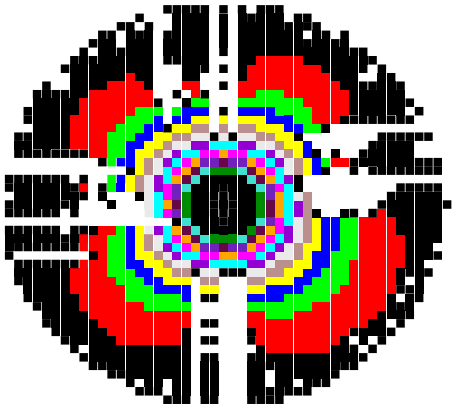

FIG. 7. (Color online) The pressure map in a plane plate geometry after 6 time steps. Zero pressure outside the pattern and within the fingers is shown in white. The pressure becomes more and more negative as one moves toward the center. Different adjacent colors (shades) represent regions with a different range of pressure. A finite number of colors is used and the sequence is repeated, so same color does not necessarily mean same pressure.

At a glance Fig. 7 shows that the fingers formed look quite realistic, when compared with experimental results shown for the plane plates in Fig. 1. The initial broadening and later tapering nature of the fingers is reproduced, as is the suppression of several fingers due to screening. The square lattice used in the simulation, makes the finger boundaries somewhat artificially jagged at some places. Smoother contours may be obtained by taking larger systems with a finer mesh of points, thus requiring more computer memory.

B. Grooved plate

The groove diameter for the circular groove and the side for the square groove are chosen to be 16. For smaller values, the effect of the groove is much less noticeable, and for larger values, it comes too close to the periphery.

In the present paper, we stop the simulation as soon as the groove is reached, the study can be extended to let secondary fingers proceed from the groove to the center. Multiple grooves as shown in Fig. 1(C) can also be introduced in future. However, for the present simple case, results are already quite interesting. Figures 8 and 9 show the simulated pressure distributions for the plate with a square and a circular groove, respectively.

On comparison with the simulated *grooved* patterns, Figs. 7 and 9 with B and C in Fig. 1, we see that the essential features introduced by the grooves are reproduced. The circular groove stabilizes pressure gradients and a larger number of fingers grow longer, compared to the plane plate patterns. The fingers and the grooves disturb the otherwise monotonic pressure distribution.

Difference between the square and circular grooved patterns is also noticeable. In Fig. 1, experiments show that with the circular groove, all fingers grow more or less equally, while in the square groove case, growth is favored toward the corners. This is expected, since the pressure gradients are stronger here. Looking at Figs. 8 and 9, we see that this is exactly the case in the simulation too.

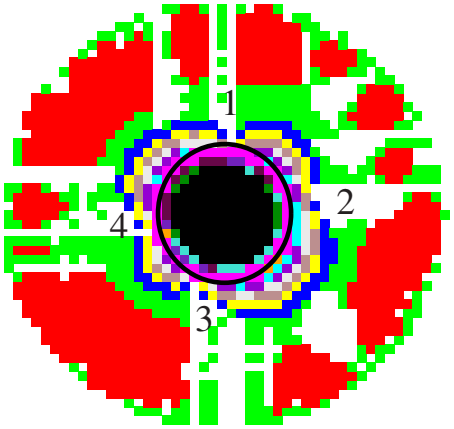

FIG. 8. (Color online) The pressure map for a circular grooved plate, after 6 time steps, after which the fingers meet the groove. Zero pressure, outside the pattern and within the fingers is shown in white. The pressure becomes more and more negative as one moves toward the center. Different adjacent colors (shades) represent regions with a different range of pressure. A finite number of colors is used and the sequence is repeated, so same color does not necessarily mean same pressure. The position of the groove is marked in black.

Figure 7 shows the pressure distribution for the plane plate during fingering. The different colors (shades) represent ranges of pressure with a difference of 1 in arbitrary units. The pressure at the center is −30.3 and it is 0 at the boundary. The white gaps are the penetrating fingers.

The simulated patterns shown have same initial conditions and all other parameters have the same value, to facilitate comparison. The time for growth is 6 time steps. The exact number of steps required to reach the center or a groove, depends of course, on the initial stochastic fluctuation at the boundary. We show patterns for the same random

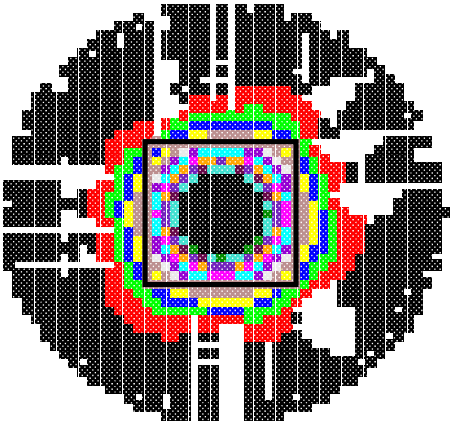

FIG. 9. (Color online) The pressure map for a square grooved plate, after 6 time steps, after which the fingers meet the groove. Zero pressure, outside the pattern and within the fingers is shown in white. The pressure becomes more and more negative as one moves toward the center. Different adjacent colors (shades) represent regions with a different range of pressure. A finite number of colors is used and the sequence is repeated, so same color does not necessarily mean same pressure. Fingers grow preferentially toward the corners of the square. The position of the groove is marked in black.

number sequence in Figs. 7–9, so that finger growth can be compared explicitly. We note that the fingers marked 1, 2, 3, and 4 in Fig. 8 which grow longest, are suppressed in Fig. 9, since they are not growing toward the corners of the square groove. Reproducibility of the essential features has been checked with several other random number sequences, these patterns are not shown here.

In the simulated figures it looks as if there are isolated air pockets within the fluid, or that some of the fingers are not connected to the air outside. However this is not the true situation, the reason is that the initial indentations at the boundary are produced in the polar coordinate picture, where the number of points is 24×360. When mapped onto the square lattice with a much lower number of points, some of the sites occupied by air are lost.

An exact comparison between simulation and experiment is rendered difficult by the fact that the extra fluid and larger depth at the grooves has not been taken into account. Assumption that the same volume of fluid with and without grooves will produce an initial blob with the same radius cannot be true in reality.

VI. CONCLUSIONS

To conclude, the complex viscous fingering process with grooved plates, can be generated by a simple computer algorithm. It appears that the major effect of the grooves is manifested through a redistribution of pressure, rather than a local change of depth. Another effect is the change in speed of finger growth [11].

Studies on viscous fingering in different conditions and with different fluids have been reported. Fingering in LHSC with ferrofluids [22] and liquid crystals [23] have also been done. Viscous fingering with anisotropy has been simulated in [10], but that is for the normal HS with a network pattern. The current attempt at simulating fingering with etched plates in the LHSC shows encouraging results.

ACKNOWLEDGMENTS

Authors are grateful to DST for supporting this work, through R/P Grant No. SR/S2/CMP-22/2004. S.S. thanks DST for a research grant.

[1] H. J. S. Hele-Shaw, Nature (London) **58**, 34 (1898).
[2] T. Vicsek, *Fractal Growth Processes* (World Scientific, Singapore, 1989).
[3] M. Daoud and H. Van Damme, in *Soft Matter Physics*, edited by M. Daoud and C. E. Williams (Springer-Verlag, Berlin, 1999).
[4] E. Ben-Jacob, R. Godbey, N. D. Goldenfeld, J. Koplik, H. Levine, T. Mueller, and L. M. Sander, Phys. Rev. Lett. **55**, 1315 (1985).
[5] J. Bohr, S. Brunak, and T. Norretranders, Europhys. Lett. **25**, 245 (1994).
[6] C Gay and L Leibler, Phys. Today **52** (11), 48 (1999).
[7] S. Roy and S. Tarafdar, Phys. Rev. E **54**, 6495 (1996).
[8] Y. Couder, F. Argoul, A. Arneodo, J. Maurer, and M. Rabaud, Phys. Rev. A **42**, 3499 (1990).
[9] A. G. Banpurkar, A. S. Ogale, A. V. Limaye, and S. B. Ogale, Phys. Rev. E **59**, 2188 (1999).
[10] J.-D. Chen and D. Wilkinson, Phys. Rev. Lett. **55**, 1892 (1985).
[11] S. Sinha, S. K. Kabiraj, T. Dutta, and S. Tarafdar, Eur. Phys. J. B **36**, 297 (2003).
[12] R. Toussaint, G. Lovoll, Y. Meheust, K. J. Maloy, and J. Schmittbuhl, Europhys. Lett. **71**, 583 (2005).
[13] S. Sinha, T. Dutta, and S. Tarafdar, Eur. Phys. J. E **25**, 267 (2008).
[14] M. Tirumkudulu, W. B. Russel, and T. J. Huang, Phys. Fluids **15**, 1588 (2003).
[15] S. K. Thamida, P. V. Takhistov, and H. C. Chang, Phys. Fluids **13**, 2190 (2001).
[16] K. V. McCloud and J. V. Maher, Phys. Rep. **260**, 139 (1995).
[17] M. Ben Amar and D. Bonn, Physica D **209**, 1 (2005).
[18] A. Lindner, D. Derks, and M. J. Shelley, Phys. Fluids **17**, 072107 (2005).
[19] W. H. Press, S. A. Teukolsky, W. T. Vetterling, and B. P. Flannery, *Numerical Recipes in Fortran F77: The Art of Scientific Computing* (Cambridge University Press, Cambridge, England, 1986).
[20] J. D. Jackson, *Classical Electrodynamics*, 3rd ed. (Wiley-India, New Delhi, 2007).
[21] S. K. Kabiraj and S. Tarafdar, Physica A **328**, 305 (2003).
[22] R. M. Oliveira and J. A. Miranda, Phys. Rev. E **73**, 036309 (2006).
[23] V. K. Horvath, J. Kertesz, and T. Vicsek, Europhys. Lett. **4**, 1133 (1987).